Journal of the Australian Ceramic Society (2021) 57:625–633
https://doi.org/10.1007/s41779-021-00568-3

RESEARCH

Investigation on physicochemical properties of graphene oxide/nano-hydroxyapatite composites and its biomedical applications

Zebin Yang[1] · Jitao Liu[1,2] · Jinkun Liu[1] · Xiliang Chen[1] · Tingting Yan[1] · Qinghua Chen[1]

Received: 4 May 2020 / Revised: 12 November 2020 / Accepted: 14 January 2021 / Published online: 23 January 2021

Abstract

Graphene oxide/nano-hydroxyapatite (GO/nHAP) composites were synthesized by simultaneous titration method. The GO powder was uniformly dispersed ultrasonically in a solution containing $Ca(NO_3)_2$. It was co-titrated with $(NH_4)_2HPO_4$, during which $NH_3{\cdot}H_2O$ was used to maintain pH of about 10. Transmission electron microscopy (TEM) showed that HAP had a drusy acicular crystal structure with 100–200 nm length in the composite. The Ca^{2+} ions were attracted by the negatively charged oxygen functional groups present on GO sheets. They also oriented the growth of hydroxyapatite preferentially along (112) plane, which was also consistent with X-ray diffractometry (XRD) results. According to X-ray photoelectron spectroscopic (XPS) results, the peak intensities of the C–O and C–C groups increased in the GO/nHAP composite. However, the number of –COO– and C–O–C groups was reduced as well as the position of peaks shifted due to electrostatic interactions. These results were also corroborated with Fourier transform infrared spectroscopy (FTIR). MTT assay indicated that GO/nHAP composites had a significant effect on proliferation of 293T cells and good biomimetic mineralization as shown by in vitro bioactivity assays. EDS spectroscopy confirmed that the Ca/P ratio in calcium phosphate deposits was 1.62, which was close to the ratio of 1.64 in natural bone. The biological performance of GO/nHAP composite proved it to be a promising candidate for bone regeneration and implantation.

Keywords Graphene oxide · Nano-hydroxyapatite · Composite · Simultaneous titration · Biocompatibility

Introduction

Hydroxyapatite (HAP) is the main inorganic component of natural bone, and it can spontaneously form a bioactive bone-like apatite at the interface of implant and bone tissue. The apatite can chemically bond with both, the implant and bone tissue, which further induces the growth of new bone via agglomeration and absorption of biological moieties. Synthetic hydroxyapatite exhibits good biocompatibility, bioactivity, and osteoconduction [1, 2]. However, the inherent brittleness, low wear resistance, poor fracture toughness, and other shortcomings limit its applications as an ideal bone replacement for long-term implantation in humans [3]. Therefore, modification of synthetic hydroxyapatite with reinforcement materials, such as polymers [4], ceramics [5], and carbon nanotubes [6], is necessary to improve its performance and increase its applicability.

Graphene oxide (GO) is a graphene derivative, which has excellent properties similar to that of graphene [7, 8]. The excellent mechanical strength of GO makes it a good candidate for biomedical implant and as a filler or reinforcing agent in tissue engineering [9]. Since GO also has good antibacterial properties [10, 11], it has been used as surgical dressing to prevent infection and heal external wounds [12]. Moreover, a stable structure built by planting phospholipid bilayer on GO [13] can promote cell adhesion [14] and proliferation [15]. Many reports suggest that GO is biocompatible [16] and biostable [17] and hence serves as an interesting platform for biomedical applications [18, 19]. More importantly, its large specific surface area and two-dimensional planar structure [20], with a large number of carboxyl, epoxy, hydroxyl, and

✉ Qinghua Chen
847501438@qq.com

[1] Faculty of Material Science and Engineering, Kunming University of Science and Technology, Kunming 650093, People's Republic of China

[2] Yunnan Baiyao Group Co Ltd, Kunming 650093, People's Republic of China

other highly active functional groups present on the surface, make it easier to combine with other substances for developing new composites through chemical bonding [21–23].

Graphene oxide-hydroxyapatite (GO/HAP) composites show higher osseointegration ability, biocompatibility, and excellent bone cellular proliferation induction with surrounding tissue [24–27]. Compared with pure HAP, the elastic modulus of GO/HAP composites was increased by 40%, in which grain bridging effect and crack deflection at the GO/HAP interface were the key factors responsible for the strengthening mechanism [26]. Recent reports have suggested that GO combined with HAP nanoparticles can enhance the cell viability and proliferative properties of osteoblasts [28, 29]. Oxygen-containing functional groups on the GO/HAP composite surface contribute to formation of interfacial bonds and homogeneous dispersion, which are also beneficial for the growth of nanosized hydroxyapatite. Besides, according to another report, oxygen-containing functional groups serve as effective nucleation sites for precipitation of Ca^{2+} ions. Their contents and distribution have an influence on the subsequent nucleation and growth of hydroxyapatite, as well as on the interfacial bonding to the support [25]. However, nanoscale HAP can grow on reduced graphene oxide, which lacks oxygen-containing functional groups, simply by tuning the precipitation condition itself [26]. This is an intriguing case, wherein the bioactive behavior of the developed composites is unknown. Hence, there is a need for systematically studying the influence of type and density of oxygen functionalities of a given type of carbon nanomaterial on the self-assembled growth of HAP, its integration onto the support, as well as its effect on the bioactivity of the respective composites.

GO/nHAP composites were synthesized by simultaneous titration method. Scanning electron microscopy (SEM), transmission electron microscopy (TEM), FTIR spectroscopy, X-ray diffractometry (XRD), and X-ray photoelectron spectroscopy (XPS) were employed to explore the morphology, crystalline size, and interfacial bonding of HAP with GO. Furthermore, the biological performance of GO/HAP composites was assessed by cellular viability test (MTT) and biomineralization assays. Based on the results of structural evaluation and biological performance of GO/HAP composites, its potential as a key material of 3D scaffold for bone tissue engineering was verified.

Materials and methods

Materials

All the chemical reagents used for the preparation and analyses, in this research work, were of analytical grade. Among them, H_2SO_4, $KMnO_4$, $NH_3{\cdot}H_2O$, $Ca(NO_3)_2{\cdot}4H_2O$, $(NH_4)_2HPO_4$, and H_2O_2 were supplied by Chengdu Kelong Chemical Industry Co. Ltd. Pristine graphite powder (500 mesh) was obtained from Qingdao Teng Shengda Carbon Machinery Co. Ltd. All the sources for preparing simulated body fluid (SBF) were offered by Hangzhou Sijiqing Biological Engineering Materials Co. Ltd. Dulbecco's modified Eagle's medium (DMEM), dimethyl sulfoxide (DMSO, analytical grade), trypsin–EDTA solution, and 3-(4,5-dimethyldiazol-2-yl)-2,5-diphenyl tetrazolium bromide (MTT, guaranteed reagent) were purchased from Shanghai Wei Macro Biological Technology Co. Ltd., whereas fetal bovine serum (FBS) was purchased from Chengdu Biomedical Technology Co. Ltd.

Synthesis of graphene oxide

GO was synthesized according to modified Hummers' method [30]. Pristine graphite powder (2 g) and concentrated H_2SO_4 (50 mL) were added into a three-necked flask, placed in an ice-water bath, and stirred for 1 h. $KMnO_4$ (10 g) was gradually dropped into the mixture. After stirring for 30 min, the bath temperature was slowly raised to 35 °C and stirred until the mixture turned brown. Then the temperature was slowly raised from 35 to 80 °C, when the brown colored reaction mixture changed its color to dark green, after which deionized water (120 mL) was slowly added. Subsequently, H_2O_2 (20 mL) was rapidly added, and the color of the suspension changed from dark green to bright yellow. Thereafter, the obtained suspension was dialyzed against distilled water for 3 days using a dialysis membrane and then dispersed ultrasonically at 250 W power (Shanghai Kedao Co. Ltd.) for 180 min. The product was finally dried to obtain graphene oxide as powder.

Synthesis of GO/nHAP composites

The graphene oxide/nano-hydroxyapatite (GO/nHAP) composite was prepared using a procedure, similar to the one described by Prabhu [31] by simultaneous titration method. Synthetic graphene oxide powder (0 and 0.01 g) and $Ca(NO_3)_2{\cdot}4H_2O$ (1.77 g) were added in a flask containing distilled water (200 mL) and dispersed ultrasonically at room temperature for 1 h to obtain 0% GO and 1 wt% GO of GO/nHAP composites, respectively. Then the suspension was further kept stirred for 0.5 h at 37 °C. $(NH_4)_2HPO_4$ (0.59 g) dissolved in deionized water (100 mL) was slowly titrated into the above suspension over 2 h. During the titration, 30% of ammonia solution was added to maintain the pH of the mixture at 10 ± 0.5. After another 24 h of stirring, the suspension was aged for 24 h and washed with distilled water to remove the impurities, until the pH turned to about 7.0. Finally, the 0% GO and 1% GO of GO/nHAP composites were obtained after freeze-drying the precipitate for 24 h, respectively.

Cellular viability test by MTT

Cytotoxic assessment and evaluation of bioactivity is an effective tool in judging the biological performance of biomaterials. The MTT (3-(4, 5-dimethylthiazol-2-yl)-2, 5-diphenylterazolium bromide) assay is a common method for evaluating cell survival and growth. The method is based on the ability of succinate dehydrogenase in mitochondria of living cells to reduce exogenous MTT to the water-insoluble blue-violet crystalline formazan, which gets deposited in the cells [32]. The third generation of human renal epithelial 293T cells, transfected with adenovirus E1A gene, was chosen for determining the cell proliferation ability. The concentration of the extract liquid was maintained in the range of 0.05–0.4 g/mL by adding 10% heat-inactivated fetal bovine serum to the culture medium. The entire preparation was allowed to stand for 24 h under an atmosphere of 5% CO_2 at 37 °C. The number of 293T cells seeded into 10 μL media was 1×10^4, which was loaded in each well and distributed into the 96 wells of the culture plate and incubated for 12 h. When the cells were almost adhered, 100 μL of the extract liquid was added in each well, and the media was further incubated for another 24 h. Subsequently, 10 μL of MTT solution was slowly added into each well, and the culture plate was incubated for 4 h under an atmosphere of 5% CO_2 at 37 °C. Once the cell culturing was accomplished, the 96-well culture plate was placed on a microplate reader, and the optical density (OD) for each well was determined at 490 nm. The relative growth rates (RGR) of cells were calculated by the following equation:

$$\mathrm{RGR} = \frac{\text{Average optical density}}{\text{Negative control optical density}} \times 100\%$$

In vitro bioactivity assay

In vitro bioactivity was determined by soaking the prepared composite material in simulated body fluid (SBF). SBF acted as an inorganic physiological solution, which had components and contents similar to the inorganic part in human plasma. The ion concentrations were Na^+ (142.0 mmol/L), K^+ (5.0 mmol/L), Mg^{2+} (1.5 mmol/L), Ca^{2+} (2.5 mmol/L), Cl^- (147.8 mmol/L), HCO_3^- (4.2 mmol/L), HPO_4^{2-} (1.0 mmol/L), and SO_4^{2-} (0.5 mmol/L), and it was prepared according to Kokubo's procedure [33]. GO/nHAP composites were immersed in vials containing 10 mL SBF at 37 °C for predetermined intervals of 1 to 28 days. After immersion, the samples were gently rinsed thrice distilled water and dried at 37 °C for 12 h. The samples were designated as GO/nHAP1, GO/nHAP2, and GO/nHAP3 corresponding to storage time in SBF of 0 day, 14 days, and 28 days, respectively.

Characterization

The morphology, crystalline size, and interfacial bonding were studied by scanning electron microscope (SEM) and transmission electron microscopy (TEM). SEM images were captured using FEI model Quanta 200, whereas the TEM images were captured using JEOL JEM-2100 microscope that operated at 200 kV. The FT-IR spectra were recorded in the reflectance model in the spectral range of 500–4000 cm^{-1} on an EQUINOX-55 FT-IR spectrometer, using KBr background. Structural and compositional analyses were conducted by X-ray powder diffractometry on D/Max-220 diffractometer, using CuKα1 radiation source (λ = 0.15406 nm) that operated at a voltage of 36 kV. Measurements were carried out from 5 to 90° with a step angle of 0.02° and the scanning speed of 4°/min. X-ray photoelectron spectroscopic analysis (XPS) was used to analyze the chemical constitution of the composite using a PHI5000 Versa Probe spectrometer with a monochromatic AlK_α X-ray source (1486.6 eV).

Results and discussion

Synthesis and characterization of GO/nHAP nanostructures

The GO/nHAP composites were successfully prepared by simultaneous titration method. Figure 1 is the schematic diagram showing the nucleation process and crystal growth of nHAP on GO sheets during the synthesis of GO/nHAP composite. The basal planes of graphene oxide were decorated with a large number of oxygen-containing functional groups. The hydroxyl and epoxy groups were present on the surface, whereas and the carboxyl groups were present along the edges [34]. Acting as an anchoring site, these oxygen functional groups induced the subsequent formation of nanostructural HAP rods, which were attached to the surfaces and edges of GO sheets [35]. At the beginning of preparation reaction, GO were ultrasonically treated sufficiently for dispersion to form. Ca^{2+} ions were attracted to the GO sheets either due to the negatively charged oxygen functional groups or through ion exchange with H^+ of carboxyl groups [36]. When much number of Ca^{2+} ions assembled on the sheets, the positively charged GO began attracting the negatively charged PO_4^{3-} ions and OH^- ions. Hence, these Ca^{2+} ions linked with oxygen functional groups became the nucleation sites for the formation of hydroxyapatite. With constantly added PO_4^{3-} and OH^- ions, the generated hydroxyapatite transformed into nano-rod shaped during the course of reaction. The $NH_3 \cdot H_2O$ not only provided OH^- ions but also maintained the pH at 10 ± 0.5 during the reaction, when the reaction mixture was magnetic stirring at 37 °C and thereafter aged for 24 h.

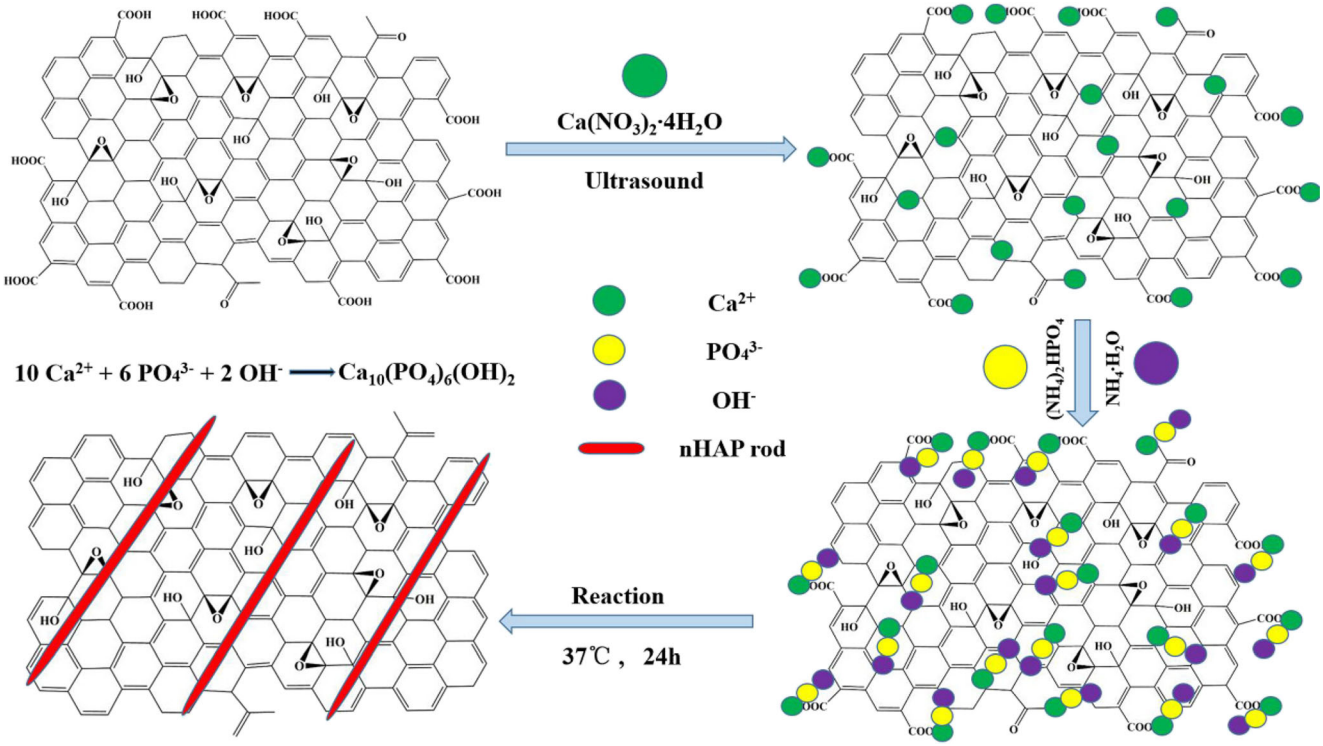

Fig. 1 Diagram for the formation process of GO/nHAP

Figure 2 shows the TEM images of GO, nHAP, and GO/nHAP composites. Figure 2 a showed the micron-scale of GO with less layers. It was evident from Fig. 2b that the hydroxyapatite crystal clusters were composed of uniformly oriented acicular nano-hydroxyapatite single crystals and some of them showed partial agglomeration. The average size of a single crystal was about 40–60 nm (length) × 5–13 nm (diameter), whereas the total length of hydroxyapatite clusters could reach to 100–200 nm. In Fig. 2b inset, the *d*-spacing was approximately 0.344 nm, which indicated that nHAP grew along the c-axis of (002) plane [37]. Meanwhile, in Fig. 2c, the length of hydroxyapatite crystal clusters was 50–100 nm, in which the nano-hydroxyapatite single crystal had dimensions of 30–50 nm (length) × 5–18 nm (diameter). In comparison of nHAP with GO/nHAP composites, the decrease in crystal size of hydroxyapatite could be ascribed to the GO sheets, which played the role of providing more number of nucleation sites for the formation of nano-hydroxyapatite crystals, thereby suppressing their growth relatively. Besides, with the addition of graphene oxide, the acicular nano-hydroxyapatite displayed a certain regularity of crystallographic orientation on the GO sheets, which could be further verified from the fast Fourier transform (FFT) results acquired at the interface between GO sheet and nano-HAP from the HRTEM image in Fig. 2d. In short, the nano-HAP showed two typical crystal lattice fringes, with lattice spacing at 0.344 nm and 0.277 nm, corresponding to (002) and (112) planes, respectively [38]. The negatively charged GO sheets strongly bonded with the positively charged nHAP through electrostatic attraction and induced it to grow along a preferred orientation of (112) plane, although nHAP alone tended to grow along the c-axis of (002) plane.

Structural information regarding GO and GO/nHAP composite are provided by X-ray diffraction (XRD) analysis as shown in Fig. 3. The appearance of Bragg reflections at $2\theta = 25.87°$, 31.77°, 32.20°, 32.90°, 34.05°, 39.82°, 46.71°, and 49.47° corresponded to the standard diffraction peaks of (002), (211), (112), (300), (202), (310), (222), and (213) planes of HAP, respectively, according to JPCDS No. 09-0432. The main diffraction peak positions of the composite material centered at 2θ matched with those of standard peaks of HAP according to JPCDS Card No. 09-0432. This confirmed that the synthesized product contained HAP, which formed the main phase of the composite. Its maximum value and its broad width indicated a small crystallite size of the hydroxyapatite nanoparticles, as shown in the systematic study of the microscopic evolution of the (211) peak. Most notably, the intensity of (112) peak was significantly increased due to increase in the intensity of the (002) diffraction peak at 25.87°. The nHAP microcrystals in the composites showed significant preferential orientations, as evidenced by variations in the intensity ratios of the three most intense peaks (300), (211), and (112) [39]. According to PDF card 09-0432, the reference intensity ratios for (002), (211), (112), and (300) were $I_{(211)}/I_{(002)} = 2.5$, $I_{(211)}/I_{(112)} = 1.67$, and $I_{(211)}/I_{(300)} = 1.67$. To quantify the texture present, the parameter R was

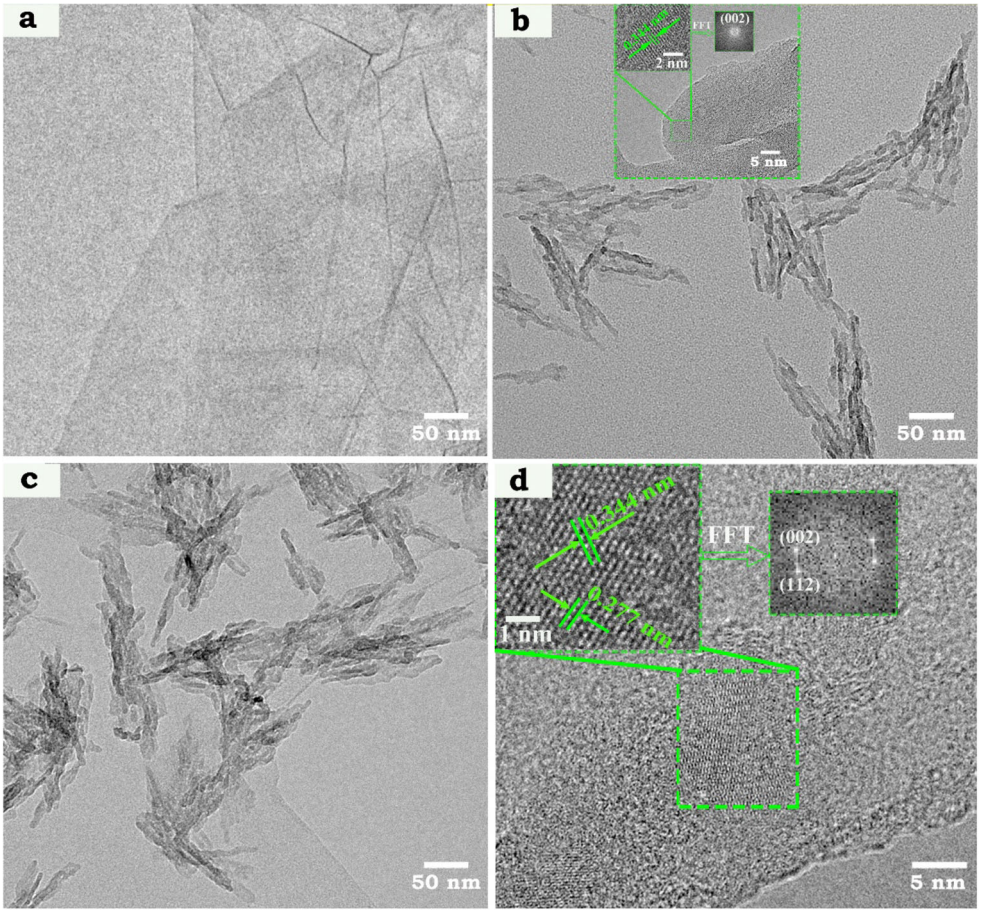

Fig. 2 TEM images of (**a**) GO and (**b**) nHAP (the inset shows the HRTEM images of nHAP) and TEM (**c**) and HRTEM (**d**) images of GO/nHAP composite

proposed [49]. The intensity ratios for (002), (300), (211), and (112) of the composites were $R_{(002)} = [I_{(211)}/I_{(002)}]/2.5 = 0.70$, $R_{(112)} = [I_{(211)}/I_{(112)}]/1.67 = 0.56$, and $R_{(300)} = [I_{(211)}/I_{(300)}]/1.67 = 0.89$. The R values of (112) planes were lower than those for (300) and (002) planes, which indicated the existence of preferred grain orientation [39]. These results proved that the hydroxyapatite crystals in the composites had preferential orientation, which tended in the direction of (112) and was consistent with the results of TEM. Finally, although the addition of graphene oxide caused broadening of the XRD peaks of the composites, it had no obvious effect on the main characteristic peaks of the composites.

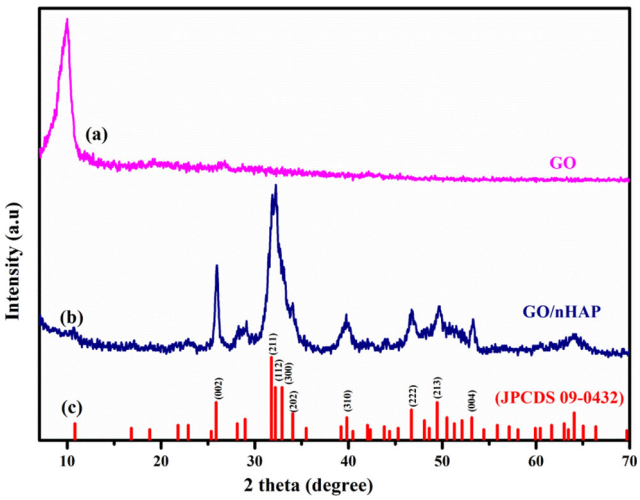

Fig. 3 XRD patterns of (a) GO, (b) GO/nHAP composite, and (c) the standard HAP (JPCDS No. 09-0432) as a reference

FTIR spectroscopy was used to determine the functional groups of the composite materials, as shown in Fig. 4. Figure 4 (a) is FTIR spectrum of nHAP, in which the absorption bands at 1250 cm^{-1}, 1030 cm^{-1}, and 573 cm^{-1} were attributed to the PO_4^{3-} in HAP [40]. Furthermore, the peaks at 3420 cm^{-1} and 1630 cm^{-1} corresponded to the characteristic –OH and H_2O stretching vibrations. The spectrum of GO (Fig. 4 (b)) showed a broad peak at around 1750 cm^{-1}, due to C=O stretching, whereas the absorption peak at 1670 cm^{-1} could be ascribed to C=C vibrations. Besides, the absorption peaks due to other functional groups such as C–OH (1350 cm^{-1}) and epoxy C–O–C (1050 cm^{-1}) groups showed up on the surface of GO. Particularly, the presence of hydrophilic functional groups increased the stability of the graphene solution which rendered the surface of the graphene oxide electronegative. It could therefore adsorb a large number of Ca^{2+} from its aqueous solution, which also contained phosphate ions, to form nucleation sites. Then, Ca^{2+} ions combined with PO_4^{3-} ions and

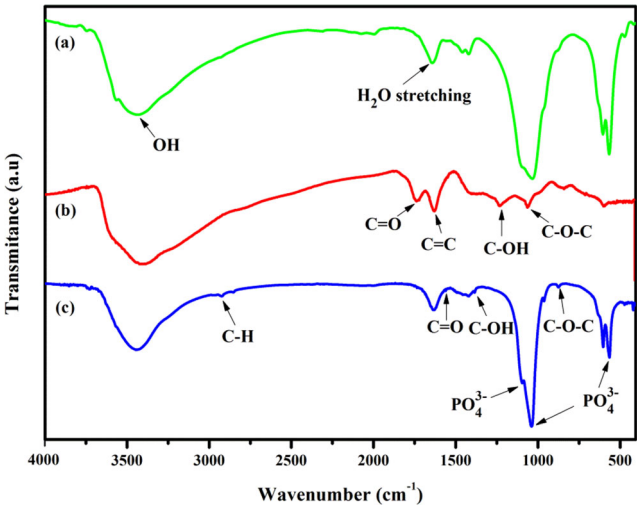

Fig. 4 FTIR spectra of (a) nHAP, (b) GO, and (c) GO/nHAP

controlled the nucleation and growth of hydroxyapatite grains. The peaks at 2852 cm^{-1}, 1595 cm^{-1}, 1380 cm^{-1}, and 875 cm^{-1} were characteristic of C–H, C=O, C–OH, and C–O–C functional groups of GO/nHAP (Fig. 4 (c)). The results of FTIR indicated shifting of wave numbers of carboxyl functional groups (such as C=O and C–OH) and epoxy (C–O–C) groups, compared to the original. Hence, it was confirmed that the GO and nHAP bonded chemically.

Figure 5 shows the XPS spectra of graphene oxide and graphene oxide/nano-hydroxyapatite. The C1s XPS spectra of GO in Fig. 5a showed four peaks centered at 288.6, 287.2, 285.9, and 284.7 eV, corresponding to –COO–, C=O, C–O, and C–C groups in GO [41]. C–C bond corresponds to the chemical bond form which by the carbon atom of the GO carbon skeleton sp^2. The C–O, C=O, and –COO– functional groups were formed in the graphite layers due to oxidation and intercalation of C–OH groups present on the edge of graphite. After reaction (Fig. 5b), the intensities of C–O and C–C peaks were enhanced, whereas peaks for –COO– and C–O–C bonds were reduced, and their positions were shirted. The peaks at 288.9, 287.6, 286.3, and 284.9 eV corresponded to –COO–, C=O, C–O, and C–C groups, respectively. The reduction in peak intensities of –COO– groups on the surface of the graphene oxide could be attributed to its interaction with the Ca^{2+} of the hydroxyapatite, which also showed a change in its electronegativity. Meanwhile, some of the C=O groups were transformed into C–O, which caused changes in peak positions and intensities of oxygen functional groups and the XPS curves. Results and conclusions of XPS analysis were consistent with the FTIR results.

MTT assay

MTT assay, which quantifies cellular mitochondrial activity in presence of a material, is commonly used to analyze the possible deleterious effects induced by the material on the cells [42]. When the relative growth rate of cells exceeds 75%, the material is qualified. However, if the relative growth rate of cells is less than 75%, the material either fails the test or requires further confirmation. The third generation of 293T cells (human renal epithelial cells transfected with adenovirus E1A gene) was chosen for detecting cell proliferation in the culture medium containing the test material. The 293T cells were seeded into the extract liquids containing nHAP and GO/nHAP with concentration gradient of 0.05–0.4 g/mL for 24 h, wherein the mass percentage of graphene oxide in the composites was 1 wt%. According to the data shown in Fig. 6, the cell number decreased with increase in concentration of extract liquid for all tested samples. For all concentration gradients of extract liquid, the total number of viable cells on GO/nHAP was always higher than on nHAP. Moreover, the relative growth rates of GO/nHAP groups were above 80% in all case, the highest being about 150%. Thus, a certain amount of graphene oxide in the composite showed a significant improvement in the proliferation of 293T cells.

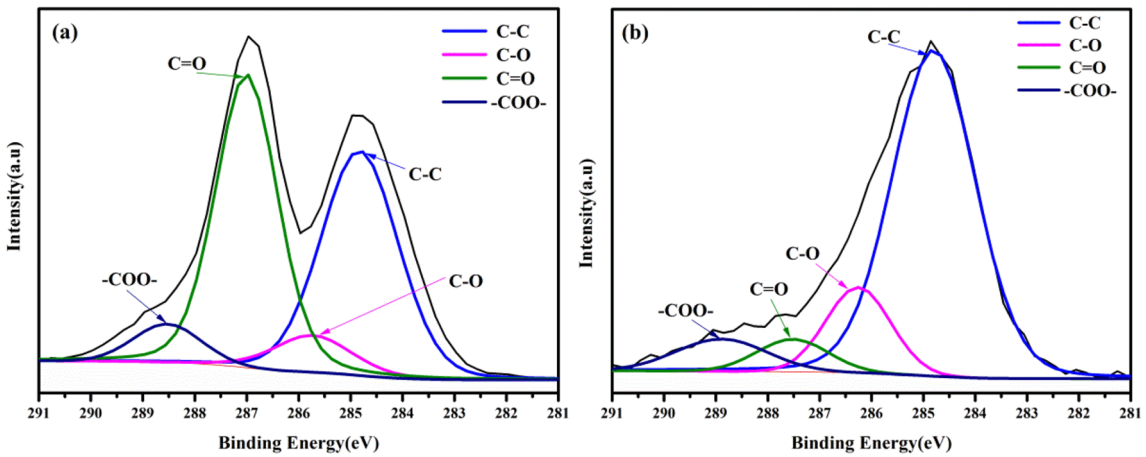

Fig. 5 C1s XPS spectra of (**a**) GO and (**b**) GO/nHAP

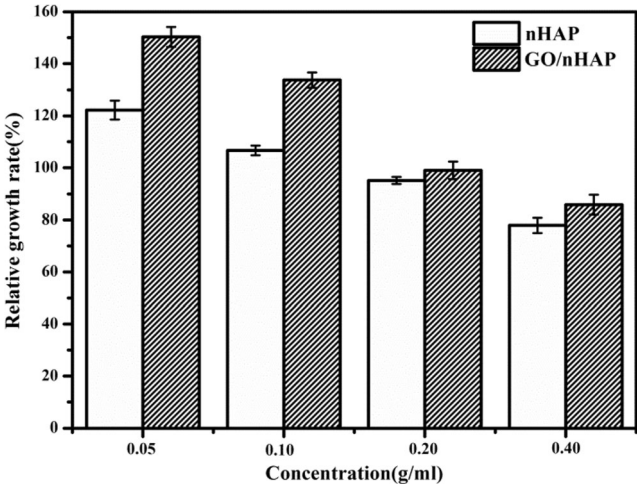

Fig. 6 Cellular proliferation analysis. The concentration of extract liquid for 0.05 g/mL, 0.10 g/mL, 0.20 g/mL, and 0.40 g/mL (the error bar represents the standard deviation)

In vitro bioactivity analysis

The use of a biological material for bone graft mainly must have two important properties: good osseointegration of it with surrounding tissues and excellent biocompatibility for promotion of growth of osteoblast cells. As one of the in vitro bioactivity assays, in vitro biomimetic mineralization is an effective way to assess the osseointegration of a material by immersing it in SBF with ion concentrations almost equal to that of human blood plasma [33]. During the in vitro biomimetic mineralization analysis, faster deposition of calcium phosphate salt on the surface of material implies good bioactivity. Figure 7 shows the SEM images of GO/nHAP composites after soaking in SBF for various time periods. Figure 7 a shows the reference sample that was not being soaked in SBF. After 14 days of soaking, some small plate-like and sphere-like deposits of calcium phosphate salt were found on the surface of material as indicated by the arrows (Fig. 7b). After soaking in the SBF for 28 days (Fig. 7c), a large number of the sphere-like deposits were found, and the size of deposits

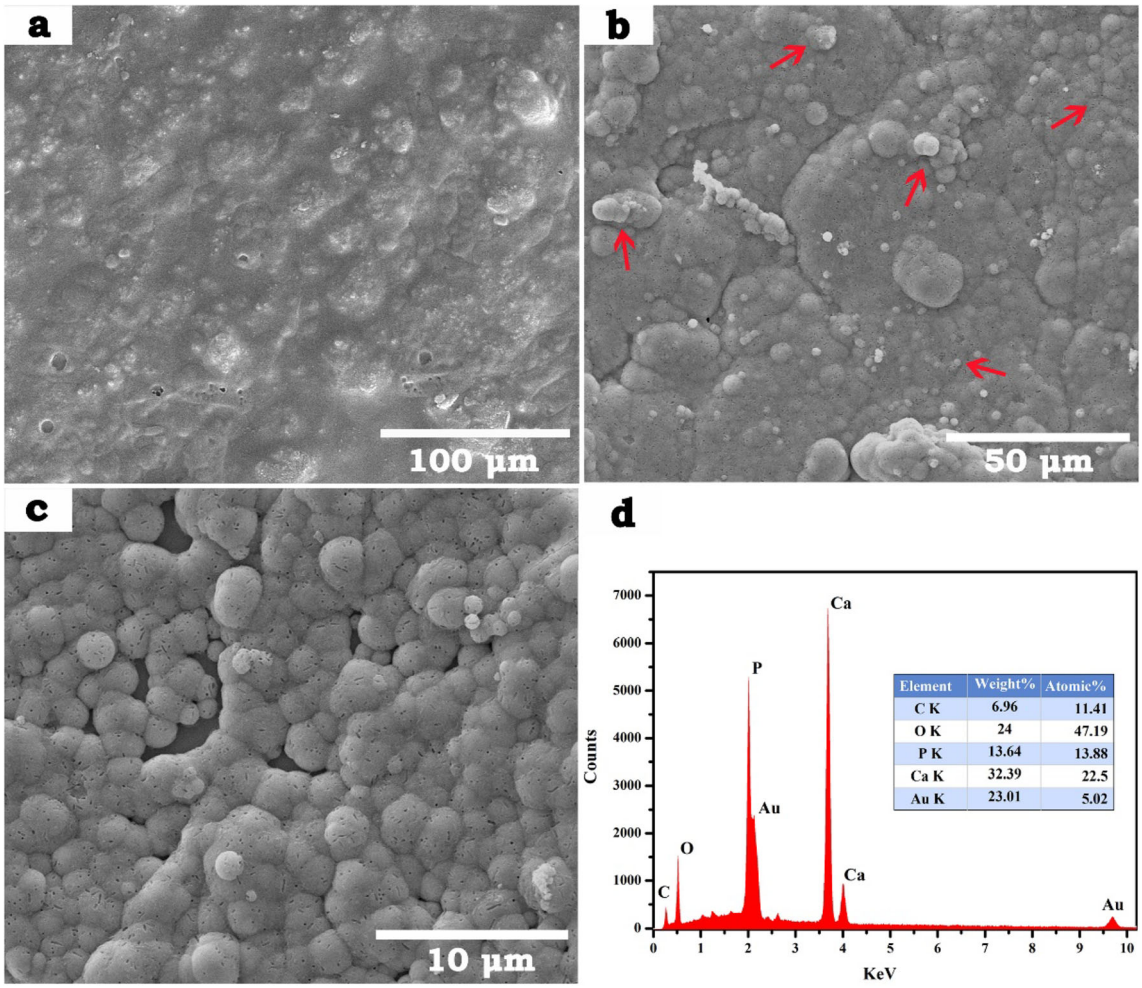

Fig. 7 SEM images of GO/nHAP composites after soaking in SBF for 0 (**a**), 14 (**b**), and 28 (**c**) days and EDAX spectra of GO/nHAP composites after soaking in SBF for 28 days (**d**)

was also increased. Figure 7 d shows the EDS spectra of calcium phosphate deposits on the surface of GO/nHAP composites, which were soaked in SBF for 28 days. The data in Fig. 7d also showed the presence of C, O, P, Ca, and Au elements, in which Au element was due to sputtering of gold on the sample during SEM analysis. Furthermore, the stoichiometric ratio of Ca/P in calcium phosphate deposits was 1.62, which was close to the stoichiometric ratio of 1.64 in natural bone tissue.

These findings were successfully indicated that nHAP modification with GO facilitates the formation of bone-like apatite on the surface of GO/nHAP composites. When GO/nHAP composites were immersed in SBF, GO could accelerate the dissolution of calcium of nHAP on the surface of GO/nHAP composites. Thus, a GO/nHAP composite was expected to have higher negative charge than pure nHAP, and the more nHAP dissolved, the more the nucleation sites were created. Moreover, the defects of the exposed GO in contact with SBF act as nucleation sites, which is evidenced by the ability of apatite formation on the surfaces of the as-received GO. Therefore, higher concentration of calcium ion in SBF and higher negative charge together with more available nucleation sites permit GO/nHAP composites to form bone-like apatite on the surface of sample [24, 27].

Conclusions

Graphene oxide/nano-hydroxyapatite (GO/nHAP) composites were successful synthesized by simultaneous titration method. The drusy acicular crystal structure of nHAP consisting of hydroxyapatite grains was effectively controlled. This hydroxyapatite grains had dimensions of about 40–60 nm (length) × 5–13 nm (diameter). During the reaction, Ca^{2+} ions were attracted onto the GO sheets due to their negatively charged oxygen functional groups and became positively charged. Now this positively charged GO attracted negatively charged PO_4^{3-} ions and OH^- ions. The Ca^{2+} ions thus adsorbed onto oxygen functional groups became the nucleation sites and oriented the growth of hydroxyapatite preferably along (112) plane. Results of XRD and TEM indicated that nHAP grew along (112) and (002) planes, but it preferred to orient along (112) plane. FTIR and XPS analyses suggested that the nHAP and the GO were linked through chemical bond. The MTT and in vitro bioactivity assays indicated that the synthesized composite had good cellular proliferation and promoted the deposition of plate-like calcium phosphate in SBF solution. The stoichiometric ratio of Ca/P in calcium phosphate salt was 1.62, which was close to the stoichiometric ratio of 1.64 in natural bone tissue. Therefore, GO/nHAP composite showed excellent potential for biomedical applications.

Acknowledgements The authors would like to thank Associate Professor Dr. Chongyan Leng for helping us with the test and analysis.

Funding The work is supported by the National Natural Science Foundation of China (No. 31260228), Education-Science Research Project for Young and Middle-aged Teachers of Yunnan (No. KKDS201551008), and Research Project of Yunnan Baiyao Group Co Ltd. (No. KKK0201651084).

References

1. Peter, O.H., Brian, J.M., George, A.B., Greg, B., Denis, D., John, A.H.: Biological responses to hydroxyapatite surfaces deposited via a co-incident microblasting technique. Biomaterials. **31**(3), 515–522 (2010)
2. Jaiswal, S., Dubey, A., Lahiri, D.: The influence of bioactive hydroxyapatite shape and size on the mechanical and biodegradation behaviour of magnesium based composite. Ceram. Int. **46**(17), 27205–27218 (2020)
3. Stankovich, S., Dikin, D., Dommett, G., Kohlhaas, K., Zimney, E., Stach, E., Piner, R., Nguyen, S., Ruoff, R.: Graphene-based composite materials. Nature. **442**(7100), 282–286 (2006)
4. Mahdavi, R., Belgheisi, G., Haghbin-Nazarpak, M., Omidi, M., Khojasteh, A., Solati-Hashjin, M.: Bone tissue engineering gelatin-hydroxyapatite/graphene oxide scaffolds with the ability to release vitamin D: fabrication, characterization, and in vitro study. J. Mater. Sci. Mater. Med. **31**(11), 97–97 (2020)
5. Belhouchet, H., Chouia, F., Hamidouche, M., Leriche, A.: Preparation and characterization of anorthite and hydroxyapatite from Algerian kaolin and natural phosphate. J. Therm. Anal. Calorim. **126**(3), 1045–1057 (2016)
6. Murugan, N., Sundaramurthy, A., Chen, S.-M., Sundramoorthy, A.K.: Graphene oxide/oxidized carbon nanofiber/mineralized hydroxyapatite based hybrid composite for biomedical applications. Mater. Res. Express. **4**(12), (2017)
7. Loh, K.P., Bao, Q., Eda, G., Chhowalla, M.: Graphene oxide as a chemically tunable platform for optical applications. Nat. Chem. **2**(12), 1015–1024 (2010)
8. Park, S., Ruoff, R.S.: Erratum: chemical methods for the production of graphenes. Nat. Nanotechnol. **5**(4), 309 (2010)
9. Amiryaghoubi, N., Pesyan, N.N., Fathi, M., Omidi, Y.: Injectable thermosensitive hybrid hydrogel containing graphene oxide and chitosan as dental pulp stem cells scaffold for bone tissue engineering. Int. J. Biol. Macromol. **162**, 1338–1357 (2020)
10. Sajjad, S., Leghari, S.A.K., Iqbal, A.: Study of graphene oxide structural features for catalytic, antibacterial, gas sensing, and metals decontamination environmental applications. ACS Appl. Mater. Interfaces. **9**(50), 43393–43414 (2017)

11. Yang, Z., Sun, C., Wang, L., Chen, H., He, J., Chen, Y.: Novel poly(L-lactide)/graphene oxide films with improved mechanical flexibility and antibacterial activity. J. Colloid Interface Sci. **507**, 344–352 (2017)
12. Dieu Linh, T., Phuong Le, T., Thai Thanh Hoang, T., Park, K.D.: Graphene oxide immobilized surfaces facilitate the sustained release of doxycycline for the prevention of implant related infection. Colloids Surf. B. **181**, 576–584 (2019)
13. Titov, A.V., Král, P., Pearson, R.: Sandwiched graphene−membrane superstructures. ACS Nano. **4**(1), 229–234 (2010)
14. Wang, L., Jia, F., Wu, D., Wei, Q., Liang, Y., Hu, Y., Li, R., Yu, G., Yuan, Q.,Wang, J.: In-situ growth of graphene on carbon fibers for enhanced cell immobilization and xylitol fermentation. Appl. Surf. Sci. **527**, 146793–146803 (2020)
15. Aidun, A., Firoozabady, A.S., Moharrami, M., Ahmadi, A., Haghighipour, N., Bonakdar, S., Faghihi, S.: Graphene oxide incorporated polycaprolactone/chitosan/collagen electrospun scaffold: enhanced osteogenic properties for bone tissue engineering. Artif. Organs. **43**(10), E264–E281 (2019)
16. Halim, A., Liu, L., Ariyanti, A.D., Ju, Y., Luo, Q., Song, G.: Low-dose suspended graphene oxide nanosheets induce antioxidant response and osteogenic differentiation of bone marrow-derived mesenchymal stem cells via JNK-dependent FoxO1 activation. J. Mater. Chem. B. **7**(39), 5998–6009 (2019)
17. Heidari, M., Bahrami, S. H., Ranjbar-Mohammadi, M.,Milan, P. B.: Smart electrospun nanofibers containing PCL/gelatin/graphene oxide for application in nerve tissue engineering. Mater. Sci. Eng. C. **103**, 109768-109776 (2019)
18. Pattnaik, S., Swain, K., Lin, Z.: Graphene and graphene-based nanocomposites: biomedical applications and biosafety. J. Mater. Chem. B. **4**(48), 7813–7831 (2016)
19. Shi, L., Wang, L., Chen, J., Chen, J., Ren, L., Shi, X., Wang, Y.: Modifying graphene oxide with short peptide via click chemistry for biomedical applications. Appl. Mater. Today. **5**, 111–117 (2016)
20. Patel, D.K., Seo, Y.-R., Dutta, S.D., Lim, K.-T.: Enhanced osteogenesis of mesenchymal stem cells on electrospun cellulose nanocrystals/poly(epsilon-caprolactone) nanofibers on graphene oxide substrates. RSC Adv. **9**(62), 36040–36049 (2019)
21. Choe, G., Oh, S., Seok, J.M., Park, S.A., Lee, J.Y.: Graphene oxide/alginate composites as novel bioinks for three-dimensional mesenchymal stem cell printing and bone regeneration applications. Nanoscale. **11**(48), 23275–23285 (2019)
22. Dinescu, S., Ionita, M., Ignat, S.-R., Costache, M., Hermenean, A.: Graphene oxide enhances chitosan-based 3D scaffold properties for bone tissue engineering. Int. J. Mol. Sci. **20**(20), (2019)
23. Zhao, Y., Chen, J., Zou, L., Xu, G., Geng, Y.: Facile one-step bioinspired mineralization by chitosan functionalized with graphene oxide to activate bone endogenous regeneration. Chem. Eng. J. **378**, (2019)
24. Li, M., Liu, Q., Jia, Z., Xu, X., Cheng, Y., Zheng, Y., Xi, T., Wei, S.: Graphene oxide/hydroxyapatite composite coatings fabricated by electrophoretic nanotechnology for biological applications. Carbon. **67**, 185–197 (2014)
25. David Núñez, J., Benito, A.M., González, R., Aragón, J.: Integration and bioactivity of hydroxyapatite grown on carbon nanotubes and graphene oxide. Carbon. **79**, 590–604 (2014)
26. Liu, Y., Huang, J., Li, H.: Synthesis of hydroxyapatite–reduced graphite oxide nanocomposites for biomedical applications: oriented nucleation and epitaxial growth of hydroxyapatite. J. Mater. Chem. B. **1**, 1826–1834 (2013)
27. Zhang, L., Liu, W., Yue, C., Zhang, T., Li, P., Xing, Z., Chen, Y.: A tough graphene nanosheet/hydroxyapatite composite with improved in vitro biocompatibility. Carbon. **61**, 105–115 (2013)
28. Prakash, J., Prema, D., Venkataprasanna, K.S., Balagangadharan, K., Selvamurugan, N., Venkatasubbu, G.D.: Nanocomposite chitosan film containing graphene oxide/hydroxyapatite/gold for bone tissue engineering. Int. J. Biol. Macromol. **154**, 62–71 (2020)
29. Fardi, S.R., Khorsand, H., Askarnia, R., Pardehkhorram, R., Adabifiroozjaei, E.: Improvement of biomedical functionality of titanium by ultrasound-assisted electrophoretic deposition of hydroxyapatite-graphene oxide nanocomposites. Ceram. Int. **46**(11), 18297–18307 (2020)
30. Hummers Jr., W.S., Offeman, R.E.: Preparation of graphitic oxide. J. Am. Chem. Soc. **80**(6), 1339 (1958)
31. Prabhu, S.M., Elanchezhiyan, S.S.D., Lee, G., Khan, A., Meenakshi, S.: Assembly of nano-sized hydroxyapatite onto graphene oxide sheets via in-situ fabrication method and its prospective application for defluoridation studies. Chem. Eng. J. **300**, 334–342 (2016)
32. Wu, T.J., Huang, H.H., Lan, C.W., Lin, C.H., Hsu, F.Y., Wang, Y.J.: Studies on the microspheres comprised of reconstituted collagen and hydroxyapatite. Biomaterials. **25**(4), 651–658 (2004)
33. Kokubo, T., Takadama, H.: How useful is SBF in predicting in vivo bone bioactivity? Biomaterials. **27**(15), 2907–2915 (2006)
34. Wang, X., Liu, Q., Liu, J., Chen, R., Zhang, H., Li, R., Li, Z., Wang, J.: 3D self-assembly polyethyleneimine modified graphene oxide hydrogel for the extraction of uranium from aqueous solution. Appl. Surf. Sci. **426**, 1063–1074 (2017)
35. Xu, C., Wang, X., Zhu, J., Yang, X., Lu, L.: Deposition of Co3O4nanoparticles onto exfoliated graphite oxide sheets. J. Mater. Chem. **18**(46), 5625–5629 (2008)
36. Dreyer, D.R., Park, S., Bielawski, C.W., Ruoff, R.S.: The chemistry of graphene oxide. Chem. Soc. Rev. **39**(1), 228–240 (2009)
37. Zhuang, Z., Fujimi, T.J., Nakamura, M., Konishi, T., Yoshimura, H., Aizawa, M.: Development of a,b-plane-oriented hydroxyapatite ceramics as models for living bones and their cell adhesion behavior. Acta Biomater. **9**(5), 6732–6740 (2013)
38. Lahiri, D., Singh, V., Benaduce, A.P., Seal, S., Kos, L., Agarwal, A.: Boron nitride nanotube reinforced hydroxyapatite composite: mechanical and tribological performance and in-vitro biocompatibility to osteoblasts. J. Mech. Behav. Biomed. Mater. **4**(1), 44–56 (2011)
39. Low, I.M.: Depth-profiling of crystal structure, texture, and microhardness in a functionally graded tooth enamel. J. Am. Ceram. Soc. **87**(11), 2125–2131 (2004)
40. Zhao, Q., Shen, Y., Ji, M., Zhang, L., Jiang, T., Li, C.: Effect of carbon nanotube addition on friction coefficient of nanotubes/hydroxyapatite composites. J. Ind. Eng. Chem. **20**(2), 544–548 (2014)
41. Weng, X., Lin, Z., Xiao, X., Li, C., Chen, Z.: One-step biosynthesis of hybrid reduced graphene oxide/iron-based nanoparticles by eucalyptus extract and its removal of dye. J. Clean. Prod. **203**, 22–29 (2018)
42. Kasputis, T., Pannier, A. K.: The role of surface chemistry-induced cell characteristics on nonviral gene delivery to mouse fibroblasts. J. Biol. Eng. **6** (2012)